JOURNAL OF MATERIALS SCIENCE 17 (1982) 3409–3422

Effect of doping elements on the morphology of graphite grown from Ni–C melts

A. MUNITZ*, S. NADIV
Department of Materials Engineering, Technion, Israel Institute of Technology, Haifa 32000, Israel

The morphology of graphite crystals grown from Ni–C melts doped with various elements was studied in detail, utilizing scanning electron microscopy, secondary ion mass spectroscopy and X-ray diffraction. Graphite crystals grown from pure Ni–C melts are normally flaky. The addition of lanthanum or calcium to the melt resulted in a tendency towards a spherical morphology, which was associated with the appearance of tiny carbide crystallites on the $\{0\,1\,\bar{1}\,0\}$ graphite surfaces. The addition of lead resulted in enhanced graphite crystal dimensions. Pyramidal-shaped tiny graphite crystallites covered the (0 0 0 1) surfaces. An approximately 20 nm thick layer of adsorbed Pb also appeared on the (0 0 0 1) surfaces. Similar effects on the morphology were obtained by the addition of sulphur (S), bismuth (Bi), antimony (Sb), or selenium (Se). The addition of La or Ca with Pb induced the growing of graphite crystals in the form of pyramids. These were covered by very tiny carbide crystallites situated on the $\{0\,1\,\bar{1}\,0\}$ faces of the graphite. The results are discussed in terms of the dopants' effects on the undercooling and growing rates in the different graphite crystallographic directions, as well as on adsorption to or interaction between the added elements and the growing graphite crystal surfaces.

1. Introduction

The morphology of graphite crystals growing during solidification of cast iron has important influence on its mechanical properties [1], hence the importance to the metallurgical industry. It was found [2] that graphite crystals growing during solidification of Ni–C melts simulates some aspects of the characteristics of cast iron. In the last few years several works have been performed on that subject [3–6]. It was established that impurities, present in the melts, have major influence on the morphology of the growing graphite crystals. Minkoff and Lux [3] classified the interaction of impurities in Ni–C melts with graphite into three categories: (a) strong interaction (as with lanthanum); (b) weak interaction (as with sulphur); (c) none at all (as with silicon). The three categories were discussed in terms of "step" and "surface" instabilities by Munitz and Minkoff [4, 5], the operative crystal growth mode depending on the amount of surface undercooling induced by the impurity [5]. A weakly reactive element is said, on adsorption, to reduce the edge energy of a step (hence the activation energy for nucleation) [7], and thereby enhance the growth rate normal to the surface [8–10]. In contrast, a strongly reactive element, reacting with the graphite through self immobilization on the (0 0 0 1) interface [11], is attached to the $0\,1\,\bar{1}\,0$ step, or even form a network, which the advancing step must traverse. Therefore, the progress is impeded or actually blocked [12]. In other words, a local high density of immobile impurity atoms may block steps moving away from a screw dislocation source, with the result, that the growth of this part of the surface is by-passed by the rest

*Present address: Nuclear Research Centre, Negev, P.O.B. 9001, Beer-Sheva, Israel.

0022–2461/82/123409–14$04.18/0

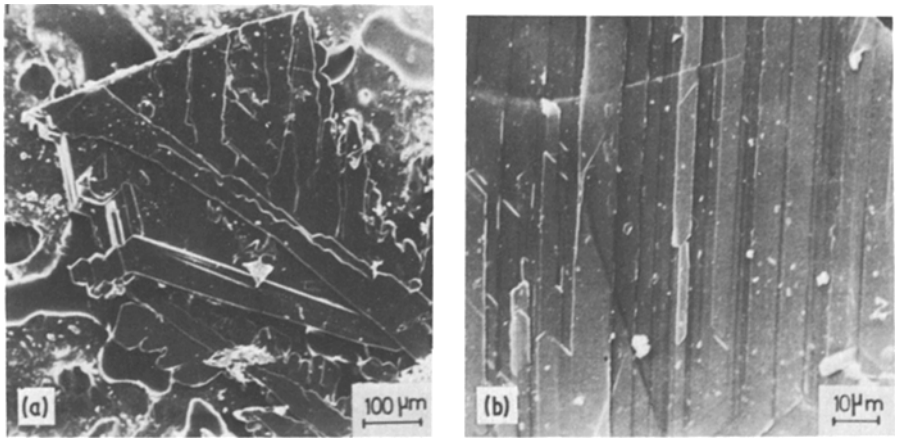

Figure 1 Secondary electron image (SEMs) of graphite crystals grown (a) from pure Ni–C solution melt, and (b) from Ni–C solution melt containing 0.35 wt % Pb.

of the crystal, and holes are formed. Such an effect was observed by Minkoff [12] in graphite crystals growing in Ni–C metallic solution containing reactive elements (such as La).

The experimental evidence supporting the model of Munitz and Minkoff [5] was restricted to only three doping elements, utilizing only scanning electron microscopy (SEM). It was thus desirable to extend the range of studied doping materials as well as to use a diversity of techniques secondary ion mass spectroscopy (SIMS), X-ray diffraction, microprobe analysis). The present work serves this need. The results suggest that atomistic considerations concerning the impurity/graphite interactions yields further understanding of the morphology of graphite crystals growing during solidification of Ni–C melts.

2. Experimental procedure

The details of sample preparation procedure were similar to those described by Munitz and Minkoff [4, 5]. Mixtures of nickel shots and the other alloying elements at chosen proportions were molten together in "semiconductor" graphite cylindrical crucibles. Lead (Pb), lanthanum (La), calcium (Ca), bismuth (Bi) and antimony (Sb) were added to the crucible in the elemental form. Sulphur (S) and selenium (Se) were added via NiS or NiSe sintered mixture. The crucible was placed in a Bridgman type furnace, and heated for 15 min at 1490° C, at which temperature the solubility of carbon in nickel is about 2.4 wt % [13]. The crucible was then pulled out of the furnace, at a rate which could be varied between 10^{-2} and 10^{-4} cm sec^{-1}.

In the course of solidification the solved carbon precipitated as primary or eutectic graphite crystals. On completion of solidification, each specimen was sectioned vertically. One half was examined metallographically, and analysed by a microprobe (JEOL type JXA 5 electron microprobe analyser). The second half was used to extract graphite crystals from small sections representative of different structural patterns. The matrix was dissolved with 1:1 aqueous solution of HNO_3 at 50° C. The collected crystals were washed carefully, dried and examined by the following methods: scanning electron microscopy (SEM, JEOL U3 scanning electron microscope); secondary ion mass spectroscopy (SIMS, AEI model IM 20 secondary ion microprobe), the primary ion beam used, constituted of oxygen (O_2) ions at impact energy 15 keV and diameter 10 μm. The resolution for secondary ion detection by the mass spectrometer was approximately 1 ppm; Debye–Sherrer X-ray diffraction analysis (Philips X-ray system). The capillary tube diameter used was 0.5 mm.

3. Results

3.1. Morphology

The morphology of graphite crystallites, which were extracted from the nickel matrix, has been studied by a scanning electron microscope (SEM).

3.1.1. Pure nickel–carbon

Graphite crystals grown from pure Ni–C solution grow in the form of thin smooth flakes, with typical large surface dimensions ranging from 0.1 to 10 mm diameter and 100 to 200 μm thickness (Fig. 1a).

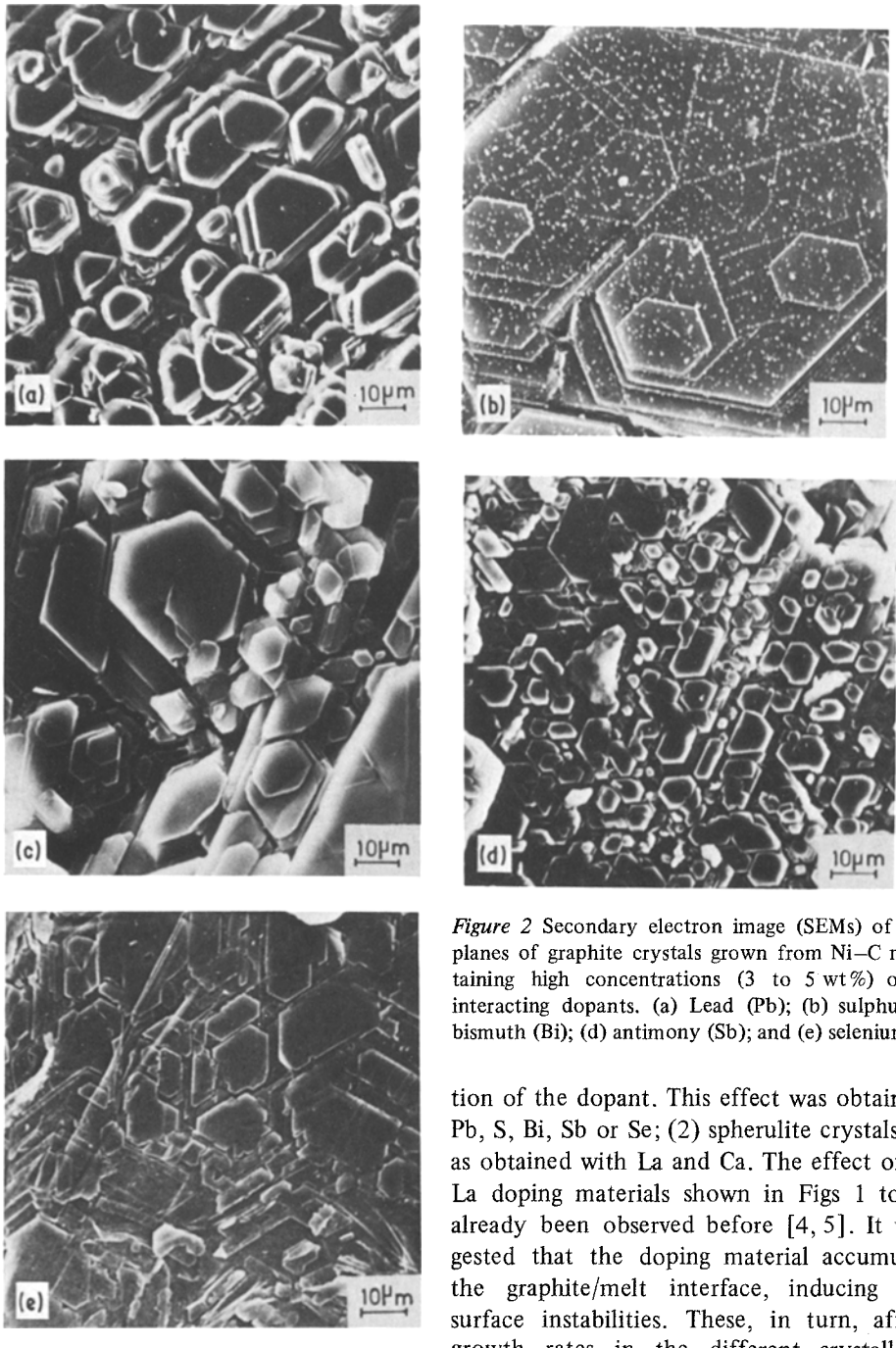

Figure 2 Secondary electron image (SEMs) of the basal planes of graphite crystals grown from Ni–C melts containing high concentrations (3 to 5 wt%) of weakly interacting dopants. (a) Lead (Pb); (b) sulphur (S); (c) bismuth (Bi); (d) antimony (Sb); and (e) selenium (Se).

3.1.2. Single element doping

Addition of dopants influences the morphology of the growing graphite crystals. Grossly, two basic morphology types were resolved: (1) flaky crystals (Fig. 2), that differ from those obtained without any doping, by the appearance of tiny pyramids on the (0 0 0 1) faces. The height and steepness of the pyramids depend on the type and concentration of the dopant. This effect was obtained with Pb, S, Bi, Sb or Se; (2) spherulite crystals (Fig. 3) as obtained with La and Ca. The effect of Pb and La doping materials shown in Figs 1 to 3 have already been observed before [4, 5]. It was suggested that the doping material accumulates at the graphite/melt interface, inducing step or surface instabilities. These, in turn, affect the growth rates in the different crystallographic directions, resulting in the observed morphology types [4, 5]. When doping materials of the "first group" accumulate at the surface, a solute boundary layer is produced. This induces constitutional supercooling at the graphite/melt interface. Low Pb concentrations (less than 0.7 wt%) cause step instabilities which result in the appearance of long laths (approximately 2 μm deep and 5 μm wide) on the (0 0 0 1) faces of the graphite (see Fig. 1b).

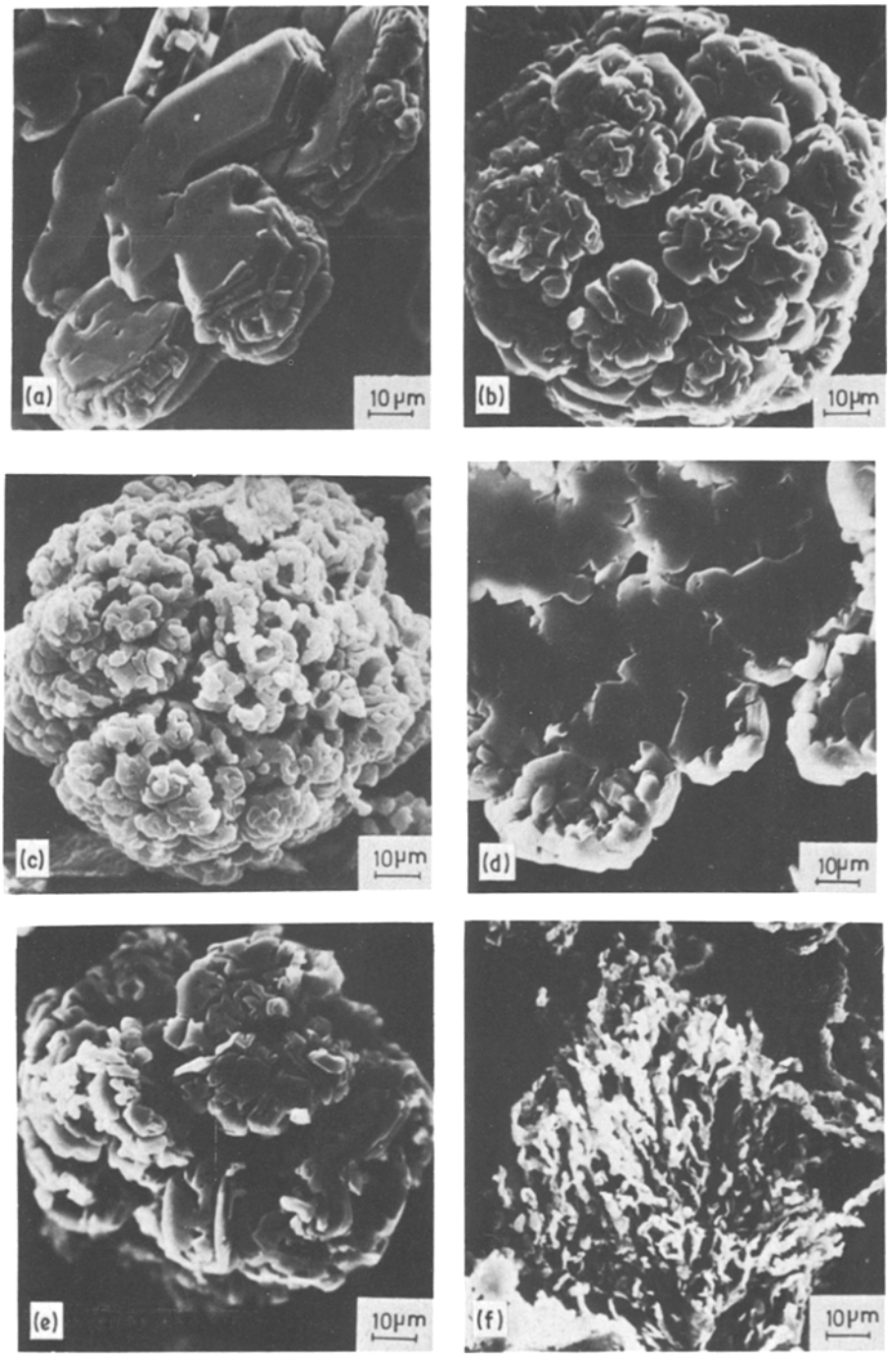

Figure 3 Secondary electron images (SEMs) of primary graphite crystals grown from Ni–C melts containing different strongly interacting dopants at various concentrations. (a) 0.2 wt % La; (b) 5 wt % La; (c) 25 wt % La; (d) 0.02 wt % Ca; (e) 0.5 wt % Ca; (f) 5 wt % Ca.

At higher Pb (as well as S, Bi, Sb or Se) concentrations (above 2 to 3 wt %), the constitutional supercooling becomes sufficient to unstabilize the (0 0 0 1) surfaces. Tiny pyramids of increasing steepness appear on the entire area of these surfaces (Fig. 2). With the "second group materials" at very low dopant concentrations (0.02 to 0.2 wt % La), the morphology resembles that of crystal grown from pure Ni–C melts. At about 0.2 wt % La, directional perturbations to the growth of

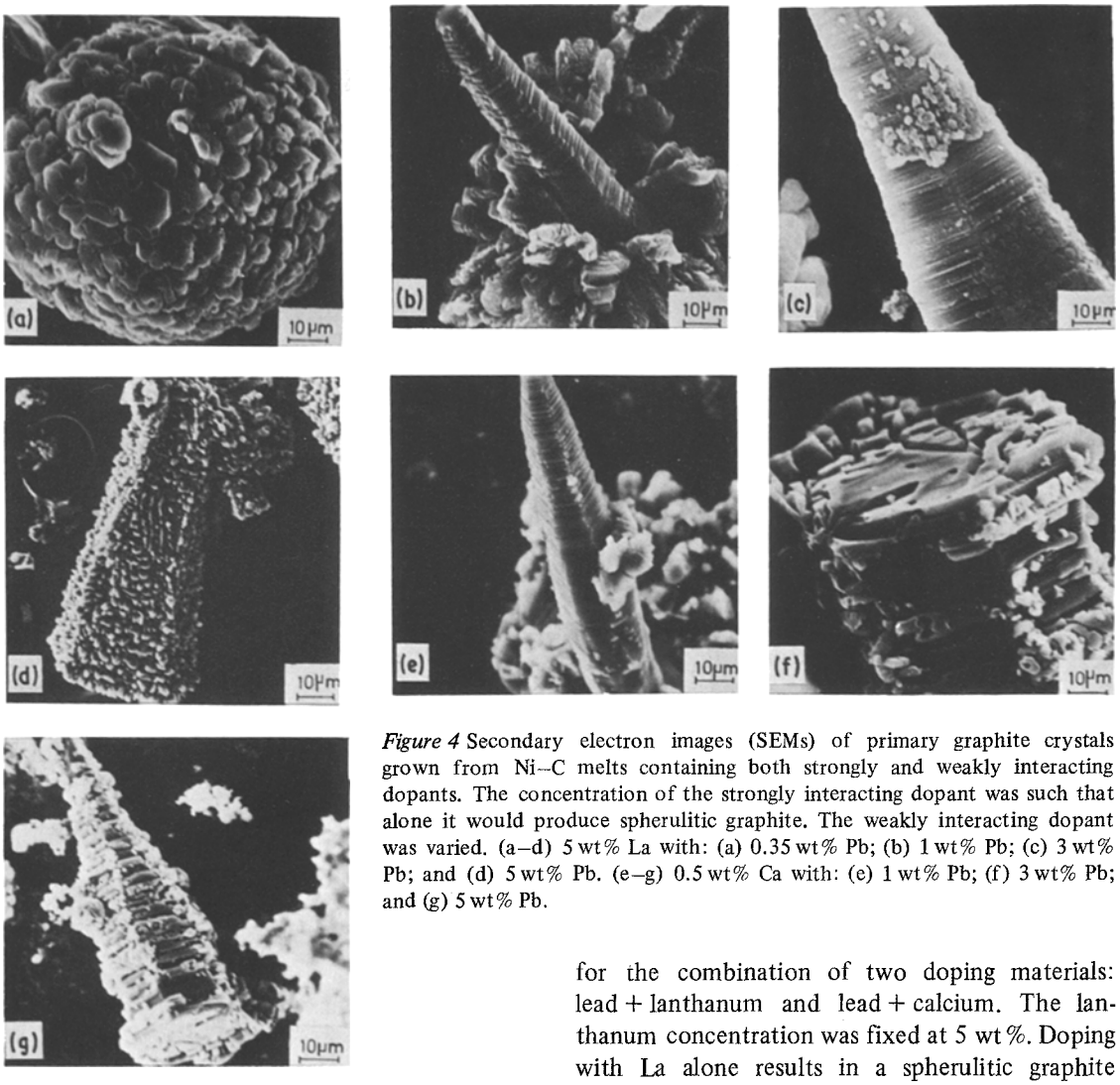

Figure 4 Secondary electron images (SEMs) of primary graphite crystals grown from Ni–C melts containing both strongly and weakly interacting dopants. The concentration of the strongly interacting dopant was such that alone it would produce spherulitic graphite. The weakly interacting dopant was varied. (a–d) 5 wt% La with: (a) 0.35 wt% Pb; (b) 1 wt% Pb; (c) 3 wt% Pb; and (d) 5 wt% Pb. (e–g) 0.5 wt% Ca with: (e) 1 wt% Pb; (f) 3 wt% Pb; and (g) 5 wt% Pb.

the $\{1\,0\,\bar{1}\,0\}$ interface were observed (Fig. 3a). At about 5 wt% La and above, all crystals became spherulitic (Fig. 3b). The dimensions of the (0 0 0 1) surfaces decreased as the La concentration increased (cf. Fig. 3a and b). Similar trend of morphology changes were seen with Ca (see Fig. 3d to f). With that doping material, however, concentrations an order of magnitude smaller are sufficient to induce similar morphology changes. Above 2 to 3 wt% Ca no graphite crystals are seen to grow. Instead, crystallites of calcium carbide start to form (Fig. 3f). The identification of the crystallites seen in Fig. 3f as calcium carbide will be discussed in Section 3.3.

3.1.3. Double element doping

In Fig. 4 we show a series of photographs taken for the combination of two doping materials: lead + lanthanum and lead + calcium. The lanthanum concentration was fixed at 5 wt%. Doping with La alone results in a spherulitic graphite shape (see also Fig. 3). The Pb content was allowed to vary between 0.1 and 10 wt%. At low Pb concentrations (0.1 wt%, see Fig. 4a) the Pb has very little effect on the morphology, and the morphology remains as with lanthanum doping alone. Increasing Pb concentration caused the spherulitic shape to disappear. Instead, graphite crystals in the form of pyramids start to grow in the [0 0 1] (c-axis) direction – see Fig. 4b. Above 3 wt% Pb, tiny crystallites appear to cover the pyramids on $\{1\,0\,\bar{1}\,0\}$ surfaces of the graphite. The density of these tiny crystallites increases with increasing Pb doping concentration (see Fig. 4). Essentially the same effects were observed with the Ca–Pb doping elements combination. Again, the Ca concentration was kept constant (0.5 wt% Ca) so as to initially provide spherulitic-shaped graphite. The Pb concentration was then allowed

to vary between 0.1 and 5 wt%, and the effect on the morphology is shown by the series of photographs in Fig. 4e to g.

3.2. Solute distribution at the graphite/matrix interface

As mentioned, the grown rods were sectioned vertically. One half was carefully polished (0.01 μm diamond paste on fine cloth soaked with kerosene), and then inserted into the electron microprobe analyser. The electron beam resolution was about 3 to 5 μm.

3.2.1. Single element doping

Results were taken with Ni–C melts doped with Pb, S and La. The crystallization sequence consists initially of primary graphite crystals. The solute is pushed out and accumulates at the graphite/molten Ni interface. Immediately afterwards, nickel with a low dopant concentration starts to crystallize. The last to crystallize should be the nickel melt containing a high dopant concentration. A considerable dopant accumulation is, therefore, expected at the graphite/matrix interface. This, indeed was verified for Pb and S, but was found false for La. In Fig. 5 are shown the results for Ni–C doped with Pb; Fig. 5a is a composition image (back-scattered electron intensity) of the inspected area; Fig. 5b and c are X-ray intensity distributions of the characteristic $L\alpha$ emission of Pb and $K\alpha$ emission of C, respectively. The bright areas in Fig. 5a result from regions of high Pb concentration (higher electron backscattering intensity due to the higher atomic number). Also, from Fig. 5b one may conclude that Pb is concentrated non-uniformly at the graphite/matrix interface. The behaviour of S is shown in Fig. 5d to f by a series of photographs similar to those shown in Fig. 5a to c. Here, however, the dopant (S) shows itself darker than the matrix (Ni) but brighter than the graphite. It is clearly seen, that the sulphur accumulates quite uniformly at the graphite/matrix interface.

As mentioned, La dopant does not accumulate near the graphite/matrix interface. This is seen in the series of photographs of Ni–C with 5 wt% La in Fig. 6. The dark area in the back-scattered electron photograph of Fig. 6a identifies graphite, the bright area identifies the lanthanum-rich alloy, and the grey area is the Ni matrix. It is clearly seen that the La distribution is not correlated in any way with the presence of graphite. The same conclusion may be drawn from the X-ray intensity images of carbon and lanthanum shown in Fig. 6b and c, respectively. A similar set of measurements were performed on a metallographic cross-section of Ni–C with 25 wt% La. While the basic behaviour was quite similar, point measurements near various tiny crystallites, that were situated near the graphite/matrix interfaces, showed correlated signals of both lanthanum and carbon. Our interpretation suggests that these tiny crystallites are, in fact, lanthanum carbides. However, the resolution was of the same order as the crystallites' dimensions, so that one could still assume that the La signal originated from La in the matrix. More conclusive evidence to clarify this point will be presented in Section 3.3.

3.2.2. Mixed elements doping

Results were taken with Ni–C doped with mixtures of La and Pb (5 wt% La and 5 wt% Pb) and of Ca and Pb (0.5 wt% Ca and 3 wt% Pb). With the mixture mentioned, the pyramidal-shaped graphite crystals were covered with additional tiny crystallites (see Fig. 4). The compositional study of the graphite and the near-by matrix for both cases is shown in Fig. 7: the La + Pb in Fig. 7a to c and Ca + Pb in Fig. 7d to f. The back-scattered electron intensity photographs indicate, once again, that no accumulation of either dopant takes place near the graphite/matrix interface. The white lines marked on both Fig. 7a and d show the scanning paths of the line profiles of Fig. 7b and c, e and f, respectively. These lines were directed to scan the tiny crystallites which surround the bulk graphite. The line profile intensities of La$L\alpha$ and C$K\alpha$ X-ray emissions are given in Fig. 7b and c, respectively. It is obvious that both La and C coexist. However, the resolution is no better than the tiny crystallites' dimensions, so one may decide that either La is accumulated near the interface, but in the matrix, or that the signal originates from lanthanum carbide, i.e. from the tiny crystallites themselves. The same effects are seen for Ca + Pb in Fig. 7d to f.

3.3. Crystal structure analysis

Crystal structure analysis of graphite crystals was performed via Debye–Scherrer X-ray diffraction analysis. Crystals grown from melts with 25 wt% La, or with 5 wt% La + 5 wt% Pb were studied. In those compositions the morphology indicated enhanced coverage of the graphite with tiny

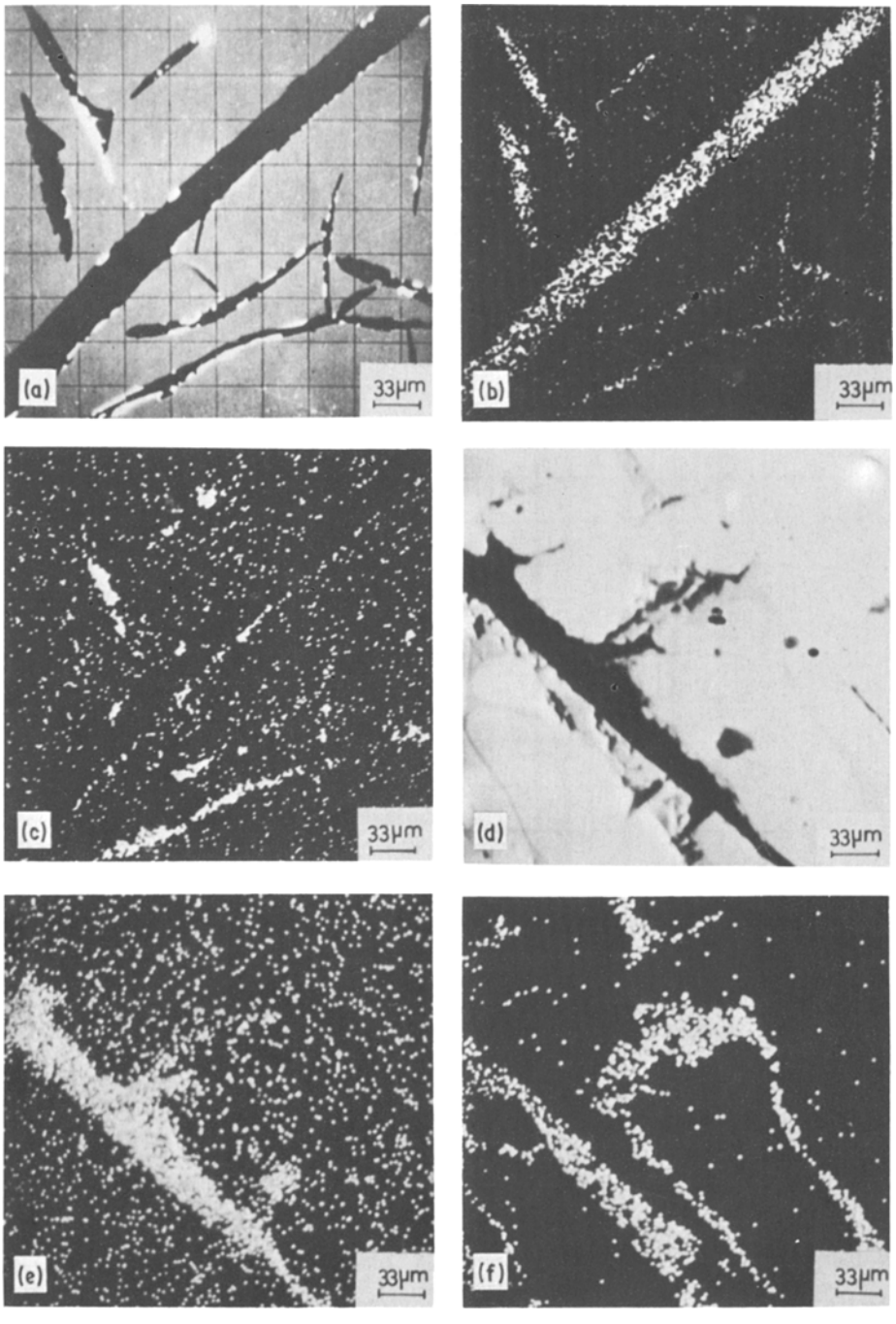

Figure 5 Elemental microanalysis of graphite and matrix for Ni–C melts doped with weakly interacting elements. (a–c): 3.5 wt % Pb. (a) Back-scattered electron image (composition image, bright zone indicates the presence of Pb). (b) X-ray emission intensity image of carbon on same surface as in (a). (c) X-ray emission intensity image of Pb on same surace as in a. (d–f): 2 wt % S. (d) Back-scattered electron image (composition image; grey zone indicates the presence of S). (e) X-ray emission intensity image of C on the same surface as in (d); (f) X-ray emission intensity image of S on the same surface as in (d).

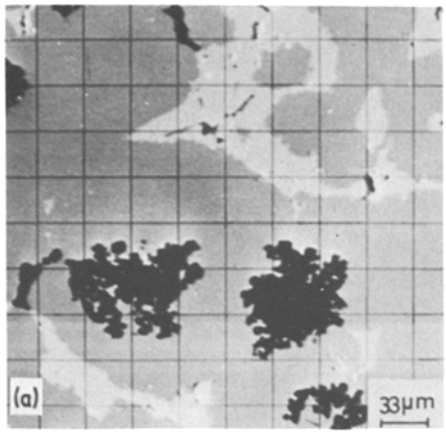

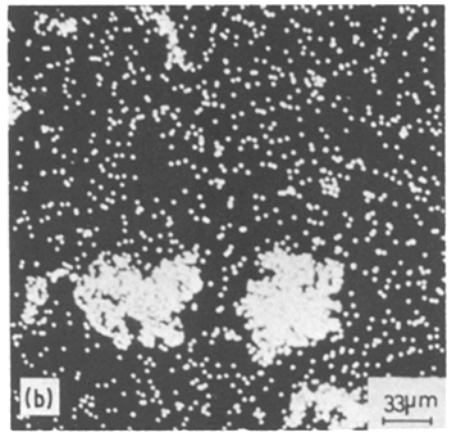

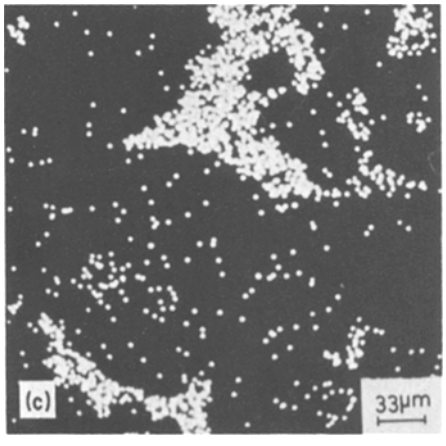

Figure 6 Elemental microanalysis of graphite and matrix for Ni–C melts doped with a strongly interacting element (5 wt% La). (a) Back-scattered electron image (composition image; bright zone indicates the presence of La). (b) X-ray emission intensity image of C on same area as in (a). (c) X-ray emission intensity image of La on the same area as in (a).

crystallites (see Fig. 4). When the Debye–Sherrer spectra of these crystals was compared to a spectrum obtained from graphite which had been extracted from pure Ni–C composition, additional lines were seen. A list of these lines is given in Table I, and is compared to the Debye–Sherrer spectrum of La_2C_3 from ASTM cards. The presence of lanthanum carbide is consistent with the correlated existence of La and C as seen by the composition analysis of the previous section (3.2). Because the atomic number of Ca is quite low, no similar analysis could be performed for Ni–C melts doped with Ca + Pb. However, the existence of calcium carbide in this case was proved separately via microprobe analysis.

3.4. Surface composition analysis

Secondary ion mass spectroscopy (SIMS) measurements were taken on the basal planes (0 0 0 1) of graphite crystals grown from either pure Ni–C melts, or melts doped with 1 wt% Pb, 1 wt% S or 0.2 wt% La. The crystals were sputtered with an O_2 beam (impact energy 15 keV), the sample thickness reduction rates being between 0.05 and 0.42 nm sec^{-1}. Emerging secondary ions were resolved by a mass spectrometer. The ion detection resolution was approximately 1 ppm. This technique has the advantage of probing the sample surface area solely (penetration depth 0.5 nm only). For comparison, in microprobe analysis the X-ray penetration depth is several microns (Section 3.2).

TABLE I Excess diffraction lines, left after the elimination of graphite lines from the Debye–Scherrer X-ray diffraction spectrum of extracted graphite crystals grown from Ni–C–25 wt% La melt

Spacing values of excess lines	Spacing values and relative intensities of La_2C_3 crystal	
(nm)	(nm)	I/I_0
0.4928	–	–
0.4290	–	–
0.3730	0.358	80
0.3450	–	–
0.3058	0.311	100
0.2788	0.278	100
0.2368	0.2343	65
–	0.2196	1
–	0.1877	35
–	0.1800	20
–	0.1751	100
–	0.1610	35
–	0.1560	1
–	0.1511	5
–	0.1430	15
–	0.1400	5
0.1360	0.1360	25

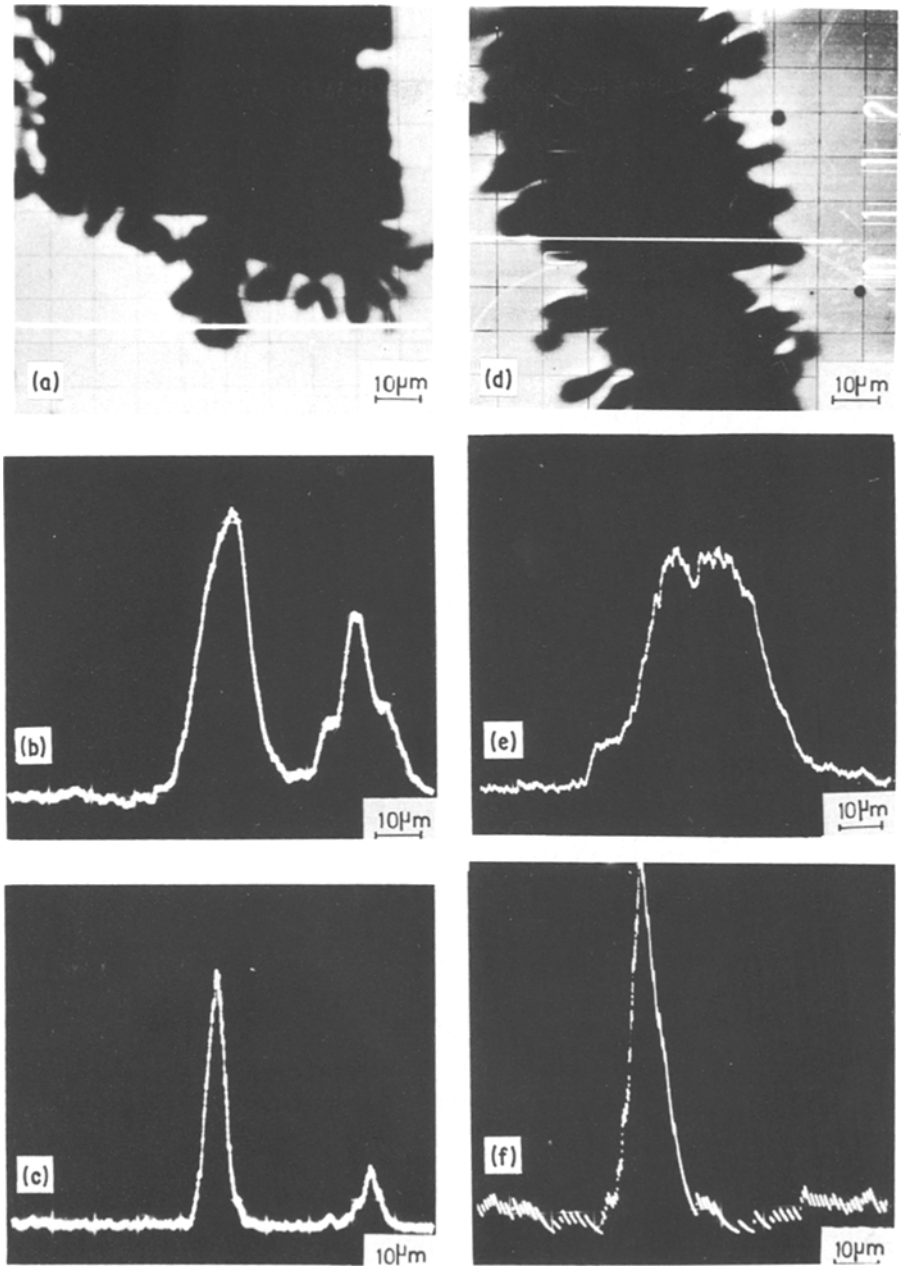

Figure 7 Elemental microanalysis of graphite and matrix for Ni–C melts containing both strongly and weakly interacting dopants. (a–c) 5 wt% La and 5 wt% Pb. (a) Back-scattered electron image (composition image). The white line indicated the path of the line profile given in (b) and (c). (b) X-ray emission intensity of C along the white line indicated in (a). (c) X-ray emission intensity of La along the white line indicated in (a). (d–f) 0.5 wt% Ca and 3 wt% Pb. (d) Back-scattered electron image. The white line indicates the path of the line profile given in (e) and (f). (e) X-ray emission intensity of C along the white line indicated in (d). (f) X-ray emission intensity of Ca along the white line indicated in (d).

Graphite crystals grown from pure Ni–C melts and those grown from the doped melts showed signals from the following elements: S, P, O, N, Na, Ti, Cr, Fe and Mg, independent of the dopant. These elements were distributed homogeneously on the surface, and as deep as 15 nm below the surface. We believe, that the effect is due to contamination caused by the extraction and preparation procedures (see Section 2), Pb or La were detected only in those crystals which were grown

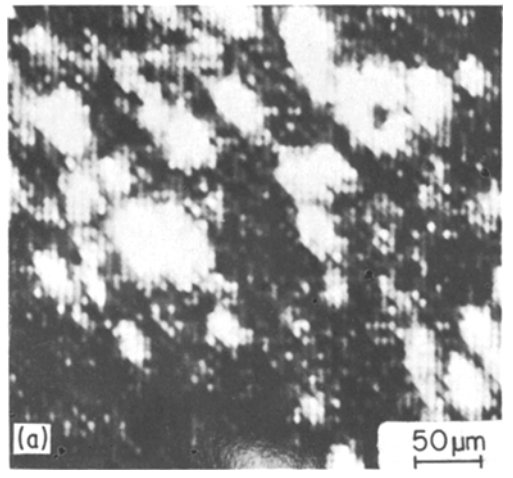

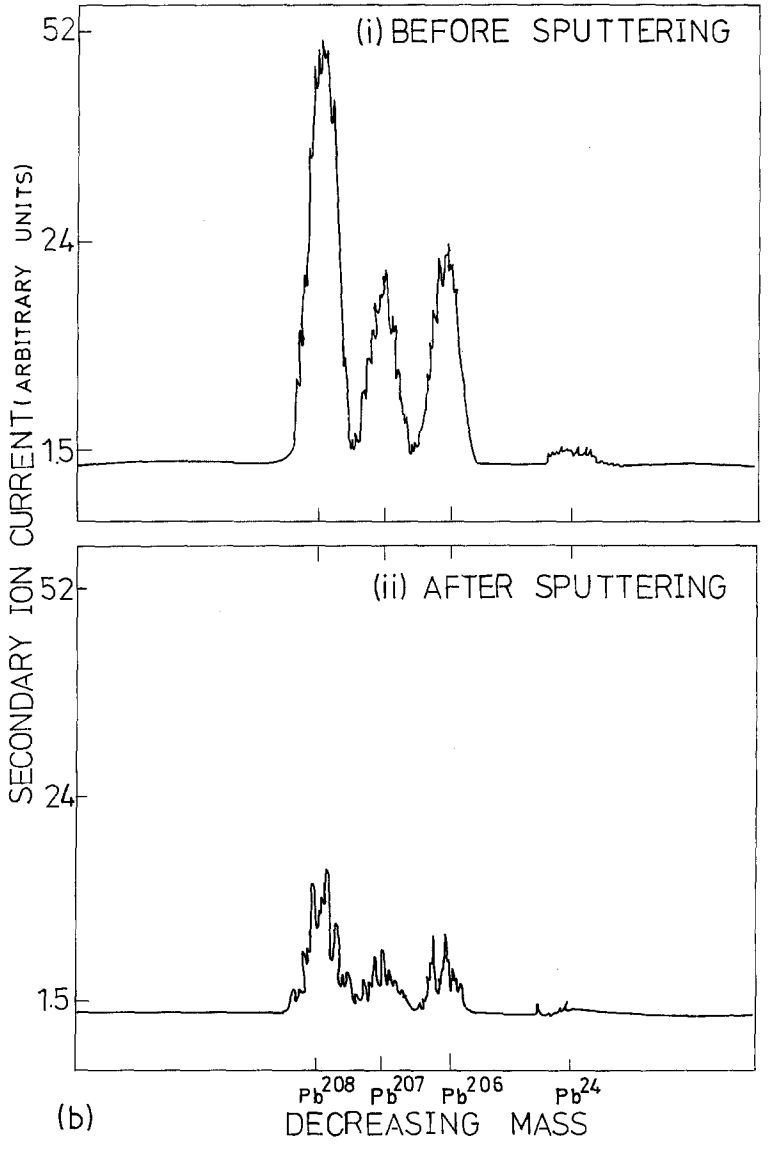

Figure 8 SIMS analysis of a graphite crystal surface grown from Ni–C 3.5 wt % Pb melt. (a) Pb^+ secondary ion image. (b) Pb^+ secondary ion mass spectrum from a surface of (i) as-extracted sample and (ii) after 1 min spattering at a rate of 0.05 nm sec^{-1}.

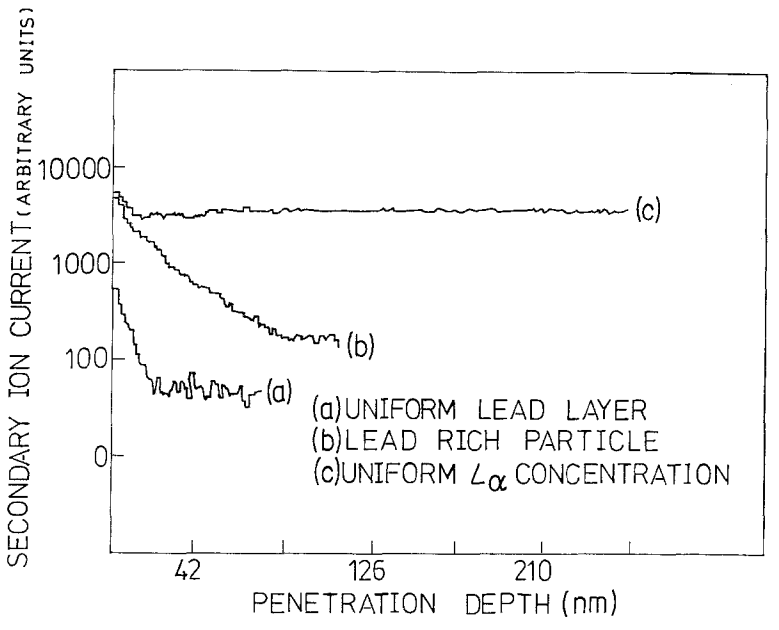

Figure 9 Profiles of secondary Pb^+ and La^+ ion intensity against depth for graphite crystals grown from Ni–C–3.5 wt% Pb melts (Pb^+ signals) and from Ni–C–0.2 wt% La melts. (La^+ signals.)

from Ni–C melts, respectively doped with Pb or La. Typical Pb^+ secondary ion image is shown in Fig. 8a, and the secondary ion mass spectrum in Fig. 8b (note that the experimental isotope ratios in Fig. 8b are in agreement with the known natural distribution $^{208}Pb:{}^{207}Pb:{}^{206}Pb:{}^{204}Pb = 52:23:24:1.5$. After 1 min sputtering, at a rate of 0.05 nm sec^{-1}, the secondary Pb^+ ion intensity signal declined (Fig. 8b). Pb^+ depth profiles are given in Fig. 9. Two types of crystal surfaces were observed: (1) those showing rapid decay of the signal (i.e. after 20 nm) and (2) those of much slower decay (i.e. after more than 100 nm). The behaviour of La is much different (Fig. 9). A plot of La^+ ion current intensity against depth is quite constant in depth over 250 nm. It appears that the La atoms adsorb on to the growing graphite crystal, immobilize themselves, and are eventually enclosed in the crystal.

4. Discussion

The theoretical considerations of Minkoff and Lux [3] provide a means of analysing the doping effect on the morphology of graphite grown from Ni–C melts. The addition of a dopant to the melt has a double role: (1) in order to initiate growth, the graphite requires enhanced undercooling; (2) dopant interaction with the graphite surface influences the growth rates. This is especially effective for reactive doping elements, and appears to be different for different growth modes. Minkoff and Lux [3] refer to the following modes: (i) growth of the $\{10\bar{1}0\}$ face by nucleation with a twist boundary; (ii) growth of the $\{10\bar{1}0\}$ face by nucleation without a twist boundary; (iii) growth of the (0 0 0 1) face by a spiral growth mechanism. In Fig. 10 we interpret our experimental situation in terms of growth curves as presented by Minkoff and Lux. Concentration changes of the same dopant affects the undercooling, ΔT, at which the crystal starts to grow. In doping materials such as Pb, S, Bi, Se and Sb, increased undercooling increases the growth rates of both modes (i) and (iii). Mode (ii) remains still ineffective. The graphite shape is determined by the ratio of the growth rates between the different crystallographic directions. The situation in this case is always $R_i > R_{iii}$, and the graphite crystals always grow in the form of flakes. The size depends on the absolute value of the growth rates, hence the undercooling, which is determined by the dopant concentration (Fig. 10a). In "strongly interacting" doping materials, such as La and Ca, one has to consider separately the low- and high-concentration limiting cases. The low-concentration limiting case is similar to the case of weakly interacting materials (Fig. 10a). This is valid for less than 0.2 wt% La or 0.02 wt% Ca. At higher concentrations, the dopant/graphite interactions are so strong as to eliminate mode (i). The dominant growth direction is now the [0 0 0 1] direction and $R_{iii} > R_{ii}$ (Fig. 10b). The crystals should then grow in the form of pyramids. In fact, we have observed spherulites (Figs. 2 and 3). This

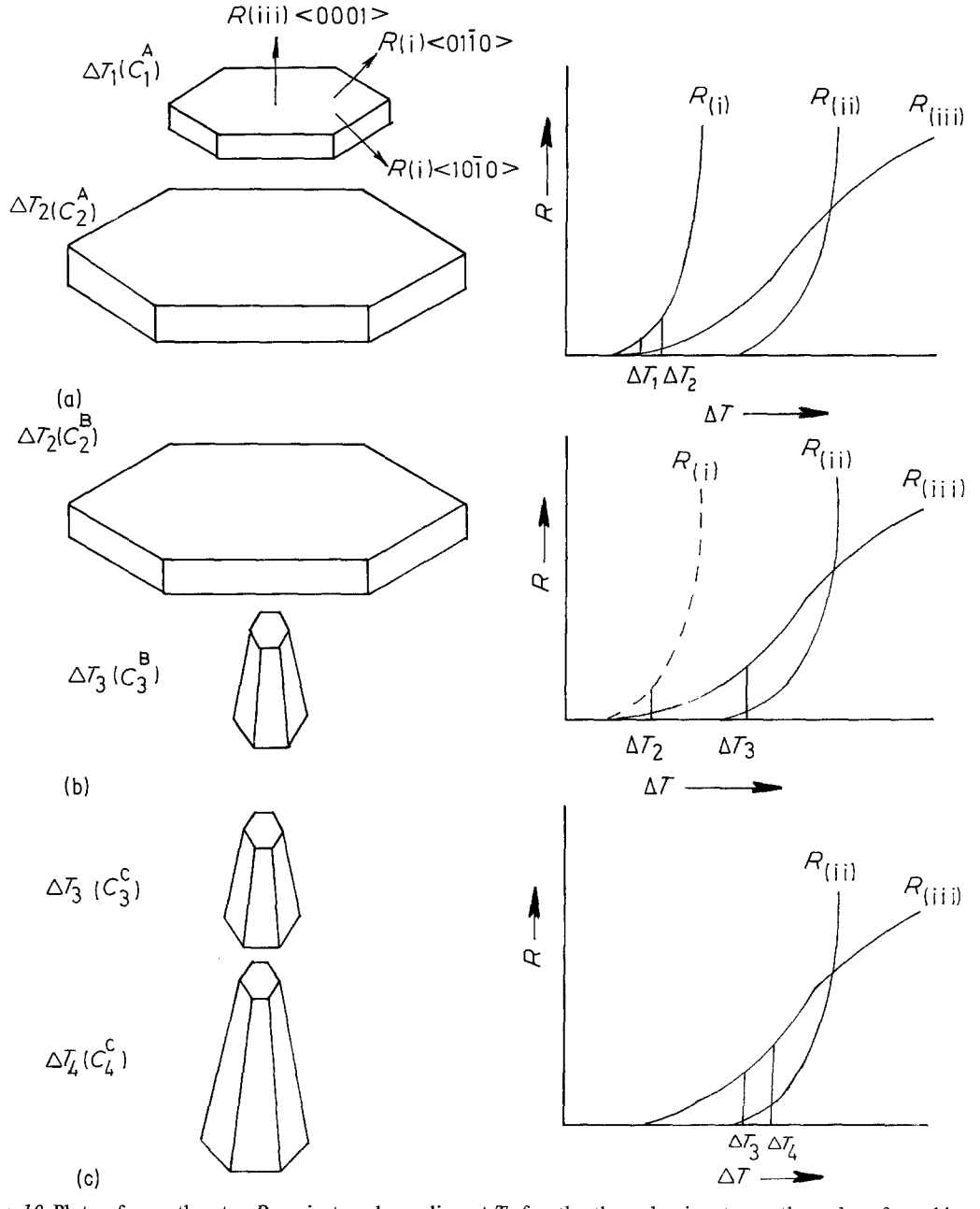

Figure 10 Plots of growth rates R against undercooling, ΔT, for the three dominant growth modes of graphite: (i) growth of (1 0 $\bar{1}$ 0) face by nucleation with twist boundary; (ii) growth of (1 0 $\bar{1}$ 0) face by nucleation without a twist boundary; (iii) growth of (0 0 0 1) face by a spiral growth mechanism. Different undercooling resulting from low or high doping concentrations labelled ΔT_1; ΔT_2; ΔT_3; ΔT_4, are marked by vertical lines. (a) Weakly interacting doping elements; concentrations $C_1^A < C_2^A$. (b) Strongly interacting doping elements; concentrations $C_2^B < C_3^B$. (c) Strongly interacting element + weakly interacting element; concentrations of weakly interacting element $C_3^C < C_4^C$. Concentrations of strongly interacting elements are constant. Expected graphite morphology for each case is shown on the left.

discrepancy will be discussed below. When a weakly interacting material is added together with a strongly interacting one, we expect a further undercooling. This is illustrated in Fig. 10c. The basic crystal shape is still a pyramid. This indeed is essentially obtained (Fig. 4). Secondary effects related to the small crystallites covering the pyramids are discussed below.

An explanation of the crystal morphologies is obtained by considering fluctuations in the

dopant densities near the graphite/melt interface. At low concentrations of weakly interacting dopants, the fluctuations occur mainly near steps on the (0001) surfaces [4, 5]. As a result, the graphite flakes appear as if covered by long lathes (Fig. 1). The crystal growth in the [0001] direction is hampered by regions of higher local dopant concentrations, effective for higher doping. The graphite basal planes are roughened by tiny pyramids that grow in the region of lower dopant concentrations (Fig. 2). Another important factor is the details of the dopant/nickel interactions. For example, the binary Ni–Pb system separates into two melts under the following conditions [13]: the temperature ranges between 1340 and 1550° C, and the Pb concentration is between 12 and 56.3 at%. This effect inherently induces variations in the Pb concentration along the graphite/melt interface, evidenced by the microprobe analysis (Fig. 5) as well as by the SIMS measurements (Fig. 9). This, in turn, produces more surface roughening. On the other hand, the binary systems Ni–S, Ni–Bi, or Ni–Sb do not separate into two melts. Therefore, the dopant concentration near the surface is more uniform, and the surface morphologies are much smoother (cf. Fig. 2a and b to 2e).

La and Ca behave as "strongly interacting" dopants. Theoretically, we would expect pyramidal-shaped graphite crystals to grow at the high doping levels. Instead, we observe the growing of spherulities. At intermediate concentrations, the graphite starts to bend through the $\langle 10\bar{1}0\rangle$ edges. SIMS analysis (Fig. 9) as well as X-ray diffraction analysis (Table I) have established the presence of lanthanum carbides in the graphite bulk or at the surface. We suggest that the bending is caused by the presence of carbide crystallites at the $\{10\bar{1}0\}$ surfaces. At 5 wt% La those carbides are responsible for successive twinning of $\{10\bar{1}0\}$ surfaces, hence the appearance of spherulites. When additional Pb is added to the 5 wt% La, the undercooling at which the crystal grows becomes so high that lanthanum carbide crystals start to grow (microprobe results, Fig. 7, shows the presence of C and La together). These completely block the growth in the $\langle 10\bar{1}0\rangle$ directions. No bending occurs, hence no spherulite may then grow, and the expected pyramids appear. These pyramids are decorated with the tiny lanthanum carbide crystals (see Fig. 4). The same effects were seen with Ca (see Fig. 4).

We will now consider the difference between "strongly interacting" elements and "weakly interacting" elements. Some literature exists on element interactions with graphite. For example, Thomas *et al.* [14], as well as Henning [15] studied the influence of structural defects on the basal plane of graphite on the nucleation of silver and gold vacuum-deposited upon the surface. Both these elements were found to migrate with great ease towards high-energy dislocation etch pits. Arthur *et al.* [16] studied the adsorption of gold and copper on the (0001) surface of graphite. These authors specified that the adsorption of the gold and copper occurs through the formation and growth of two-dimensional nuclei of mobile Au or Cu surfaces, which are weakly attached to the graphite substrate via van der Waals' forces. Such weak non-localizing bonds are consistent with the high surface mobility of Au or Cu on the surface. Some recent observations of zinc adsorbed on to GaAs [17] and cadmium on to germanium [18] indicate that this behaviour of Ag, as well as Au and Cu, on graphite is by no means unique. One may recognize that all elements performing "weak interactions" with the graphite (Pb, S, Bi, Se, Sb) belong to the right-hand side of the Periodic Table. Those performing "strong interaction" with the graphite, belong to the left-hand side of the Periodic Table (La, Ca). We suggest that this classification is general. The nature of the weak interaction is similar to that observed by Arthur *et al.* [16] for gold and copper, i.e. weak van der Waals' forces upon the (0001) surfaces. The bonding occurs via overlap of the carbon π orbitals and the dopants. This permits continuation of graphite growth. The elements capable of making σ bonding prefer the $\{10\bar{1}0\}$ surfaces, where σ orbitals are available. In the extreme of this effect, under sufficient undercooling rates, dopant carbides are formed, which completely block growth in the $\langle 10\bar{1}0\rangle$ direction. As mentioned, the intermediate case is characterized by a succession of twinning, causing the appearance of spherulites.

Recently, it has been shown using Auger spectroscopy [19], that antimony (Sb) is adsorbed at the interface of graphite nodules grown from nodular cast iron. This is similar to our own observations concerning the behaviour of Sb with respect to graphite. Furthermore, it appears that the Ni–C system may be used to simulate the graphite growth in cast iron. Indeed, Mg and Ca

are known to generate nodular graphite in cast iron, an effect similar to the spherulitic graphite grown from Ni–C with the addition of La or Ca.

5. Conclusion

The effects of added impurities on the morphology of graphite crystals growing from Ni–C melts was studied for a large variety of elements. The elements could be classified into two types according to their effects at high doping levels: (i) weakly interacting elements (Pb, S, Bi, Sb and Se, all belonging to the right-hand side of the Periodic Table); (ii) strongly interacting elements (La or Ca, which belong to the left-hand side of the Periodic Table). Both types induce undercooling at which the graphite starts to grow, hence variations in the growth rates, which are different in different crystallographic directions. At low dopant concentrations the crystals are larger, but preserve their original flaky shape. At high doping levels, type (i) elements further increase the above effects. The effect of type (ii) elements is more complicated. Apart from increasing the undercooling, the growth mode in the $(1\,0\,\bar{1}\,0)$ directions by nucleation with a twist boundary is eliminated. At the same time, growth in that direction changes angle several times due to the formation of dopant carbides. The resultant graphite shape is spherulitic. When the undercooling is accentuated by the addition of both strongly and weakly interacting elements, the crystal shape is pyramidal.

Fine details are seen on the graphite surfaces for high dopant concentrations, depending on the nature of the dopant: tiny pyramids appear on the $(0\,0\,0\,1)$ surfaces for weakly interacting dopants (type (i)). They probably result from fluctuations in dopant concentration near the graphite surface. These dopants are attracted to the (0001) surfaces via van der Waals' forces. For strongly and weakly interacting dopants added together, tiny carbide crystallites appear on the $\{1\,0\,\bar{1}\,0\}$ surfaces. This is a result of chemical reaction involving the free carbon σ bonds at the $\{1\,0\,\bar{1}\,0\}$ surfaces and the strongly interacting dopants.

Acknowledgements

The authors wish to thank Professor I. Minkoff for stimulating their interest in the present research. The SIMS analyses were performed at the Materials Research Laboratories, University of Illinois, Urbana, and thanks are due to Dr P. Williams. The authors also gratefully acknowledge helpful discussions with Dr R. Lin on surface adsorption problems. This paper in its final version was edited by Dr Z. Burshtein of Nuclear Research Centre, Negev.

References

1. A. LITTLE and H. J. HEINE, Proceedings of Second International Symposium on the Physical Metallurgy of Cast Iron, Battelle Institute, Geneva, 1974 (Georgi Publishing Co., St. Saphorin, 1975). pp. 767–788.
2. H. MORROGH and W. J. WILLIAMS, *J.I.S.I.* **155** (1974) 321.
3. I. MINKOFF and B. LUX, 2nd International Symposium on the Physical Metallurgy of Cast Iron, Battelle Institute, Geneva, 1974 (Georgi Publishing Co., St. Saphorin, 1975).
4. A. MUNITZ and I. MINKOFF, International Conference on Solidification and Casting, Sheffield, UK, 1977. Conference preprint volume, paper no. 13.
5. *Idem*, 45th International Foundry Congress, Budapest (1978).
6. I. MINKOFF, International Symposium on Quality Control of Engineering Alloy and the Role of Metal Science, Delft, Holland (Delft University Technical Publications, Delft, 1977) p. 79.
7. G. W. SEARS, "Crystal Growth and Imperfection of Crystals" (Wiley, New York, 1958) p. 411.
8. D. P. WOODRUFF, "The Solid-Liquid Interface" (Cambridge University Press, 1973) pp. 40–62.
9. M. VOLMER, "Kinetic der Phasenbildung" (Steinhaupt, Dresden and Leipzig, 1939).
10. I. MINKOFF and M. ORON, 2nd International Symposium on the Physical Metallurgy of Cast Iron, Battelle Institute, Geneva, 1974 (Georgi Publishing Co., St. Saphorin, 1975).
11. N. CABRERA and D. A. VERMILYEA, "Growth and Perfection of Crystals" (Wiley, New York, 1958) pp. 393–40.
12. I. MINKOFF, *Phil. Mag.* **12** (1965) 1083.
13. M. HANSEN, "Constitution of Binary Alloys", 2nd edn. (McGraw Hill, New York, 1958).
14. J. M. THOMAS, E. L. EVANS and J. O. WILLIAMS, *Proc. Roy. Soc. London Ser. A 1586* **331** (1972) 417.
15. G. R. HENNING, "Chemistry and Physics of Carbon", edited by P. L. Walker, Jr, Vol. 2 (Edward Arnold, London, 1966) p. 1.
16. J. R. ARTHUR and A. Y. CHO, *Surface Sci.* **36** (1973) 641.
17. J. R. ARTHUR, *ibid.* **43** (1974) 369.
18. R. J. H. VORHOEVE, J. N. CARIDES and R. S. WAGNER, *J. Appl. Phys.* **43** (1972) 4876.
19. Perkin-Elmer Corporation, *Amer. Lab.* February (1979) 11.

Received 25 September 1981
and accepted 8 May 1982